Available online at www.sciencedirect.com
SCIENCE DIRECT
Applied Catalysis A: General 309 (2006) 144–154
APPLIED CATALYSIS A: GENERAL
www.elsevier.com/locate/apcata

Chemo-, regio- and stereo-selective aerial oxidation of limonene to the *endo*-1,2-epoxide over Mn(Salen)-sulfonated SBA-15

Lakshi Saikia, D. Srinivas *, Paul Ratnasamy *

National Chemical Laboratory, Pune 411 008, India

Received 10 February 2006; received in revised form 9 May 2006; accepted 10 May 2006

Abstract

Mn(Salen) complexes immobilized on sulfonic acid-functionalized SBA-15 molecular sieves (SBA-15-*pr*-SO_3-Mn(Salen)) catalyze the Mukaiyama-type oxidation of *R*-(+)-limonene selectively to the 1,2-epoxide with molecular oxygen at 298 K (Salen = *N*,*N*-ethylenebis(salicylidenaminato)). The *endo*-diastereomer is formed with a diasteromeric excess of 39.8%. This catalyst exhibited higher catalytic activity than ''neat'' Mn(Salen) complexes directly supported on SBA-15 or zeolite-Y. A change in the oxidation state of Mn from +3 in the ''neat'' complex to +2 when immobilized on the sulfonated surface is a probable cause for the observed enhancement of catalytic activity. A part of the Mn complexes was leached out of the solid phase during the reaction.

Keywords: Aerial oxidation of limonene; Chemo-, regio- and stereo-selective epoxidation; Catalysis by Mn(Salen) complexes; Sulfonic acid-functionalized SBA-15; Immobilized Mn Schiff base complexes; Mesoporous molecular sieves; Mukaiyama-type oxidation

1. Introduction

Limonene epoxide is a key raw material in the synthesis of pharmaceuticals, fragrances, perfumes and food additives [1]. Conventionally, it is manufactured by oxidation of limonene with stoichiometric amounts of peracids. As this process is not ecofriendly, attempts are in progress to develop more suitable solid catalysts for this reaction [2–12]. Limonene is one of the molecules of choice to study chemo-, regio- and stereo-selective catalytic oxidations. Oxidation of limonene, in general, yields a variety of products. Epoxides will be the selective products if oxidation occurs at olefinic positions. If the oxidation takes place at allylic positions, the products will be carveol and carvone. In addition, limonene has two olefinic bonds (1,2 and 8,9) and the oxidation can take place at either or both of these sites. Further, two types of diastereomers (*endo* and *exo*) are expected for each of the epoxide products. Most of the known solid catalysts (Ti-MCM-41 [2], carbon-anchored $Co(acac)_2$ [10], and supported Keggin heteropoly compounds [4], for example) show significantly low limonene conversions and epoxide selectivities (20–30%); carveol, carvone and polymeric products are formed in large quantities. They require expensive oxidants such as alkyl hydroperoxides and H_2O_2. When using air as an oxidant, sol–gel-prepared Co/SiO_2 [6] yields large amounts of allylic oxidation products. Mn complexes are known to be efficient in the Mukaiyama-type of epoxidation of terpenes at mild conditions in the presence of molecular oxygen (oxidant), *iso*-butyraldehyde (co-reagent) and N-containing bases (additive) [13]. Schuster and Hölderich [7] reported the application of modified faujasite encapsulated Mn and Co complexes of (*R*,*R*)-(*N*,*N*′)-bis(3,5-di-*tert*-butylsalicylidene)-1,2-diphenylethylene-1,2-diamine for this reaction (epoxide selectivity ≅50% and diastereomeric excess (de) = 36%). Bhattacharjee et al. [11] reported the use of chiral sulfonato-salen-Mn(III) complexes entrapped in layered double hydroxide hosts (de = 31%) [11]. In this study we report the aerial oxidation of *R*-(+)-limonene over Mn(Salen) complexes immobilized on sulfonic acid-functionalized, mesoporous SBA-15 molecular sieves. These catalysts are superior to zeolite-Y encapsulated complexes (Mn(Salen)-Y) and ''neat'' Mn(Salen)Cl as well as other solid catalysts hitherto investigated for this reaction. Functionalization of the solid surface with sulfonic acid enhances the catalytic performance significantly.

* Corresponding authors. Tel.: +91 20 2590 2018; fax: +91 20 2590 2633.
E-mail addresses: d.srinivas@ncl.res.in (D. Srinivas), p.ratnasamy@ncl.res.in (P. Ratnasamy).

0926-860X/$ – see front matter © 2006 Elsevier B.V. All rights reserved.
doi:10.1016/j.apcata.2006.05.011

2. Experimental

2.1. Materials preparation

2.1.1. Preparation of SBA-15

SBA-15 was prepared [14] using tetraethyl orthosilicate (TEOS, Aldrich Co.) as silica source, Pluronic P123 (poly-(ethylene glycol)-block-poly(propylene glycol)-block-poly-(ethylene glycol), $EO_{20}PO_{70}EO_{20}$; average molecular weight = 5800, Aldrich Co.) as template and HCl as pH controlling agent. In a typical synthesis, 10 g of P123 was dispersed in 75 g of water and 300 g of 2 M HCl solution while stirring. To it, 22 g of TEOS was added over 45 min. The gel that formed was continuously stirred at 313 K for 24 h and then aged at 373 K for 48 h. Then, the solid product was separated by filtration, washed with deionized water, and dried, first at 298 K, and then at 353 K. The material was finally calcined in air at 823 K for 6 h, to decompose the triblock co-polymer P123 and to obtain a white powder, SBA-15.

2.1.2. Preparation of SBA-15-pr-SH

SBA-15-*pr*-SH was prepared according to known procedures [15] by reacting 3-mercaptopropyltrimethoxysilane (MPTMS; Aldrich Co.) with a pre-formed SBA-15. Thiol-functionalization was accomplished by condensation of MPTMS with surface silanols. In a typical preparation, calcined SBA-15 (4 g) was first activated under vacuum at 423 K for 4 h. It was then dispersed in dry-toluene (100 ml) and 5.42 g of MPTMS was added to it, in small amounts, over 10 min. The contents of the flask were refluxed, under nitrogen, for 24 h. Soxhlet extraction, initially with dichloromethane (for 12 h) and then with acetone (for 12 h), yielded the thiol-functionalized SBA-15 (hereafter referred to as SBA-15-*pr*-SH). It was dried at 353 K. The thiol loading estimated by sulfur analysis was 1.5 mmol/g.

2.1.3. Preparation of SBA-15-pr-SO_3H

To 4 g of SBA-15-*pr*-SH (activatated at 373 K), was added 65 ml of 30% aqueous H_2O_2 [16]. The mixture was then stirred for 8 h at 298 K. The solid was filtered off, washed with deionized water and dried, first at 298 K for 24 h and then at 353 K for 12 h, to obtain sulfonic acid-functionalized SBA-15 (hereafter referred to as SBA-15-*pr*-SO_3H). The content of –SO_3H functional group = 0.55 mmol/g silica (estimate based on sulfur analysis); pH measurements indicated the acidity/ion exchange capacity of the catalyst to be 0.725 mequiv./g silica, in good agreement with the estimate from sulfur analysis.

2.1.4. Preparation of SBA-15-pr-SO_3-Mn(Salen)

"Neat" Mn(Salen)Cl was prepared by known procedures [17]. Then 3 g of SBA-15-*pr*-SO_3H (activated at 353 K, under vacuum, for 2 h) was dispersed in 50 ml of dry-toluene. To it, 0.45 g of "neat" Mn(Salen)Cl complex was added. The contents were refluxed, under nitrogen atmosphere, for 24 h. Mn(Salen)Cl was not soluble instantly in toluene, but under reflux conditions it formed a brown solution. The solid silica catalyst was filtered off, dried at 333 K and Soxhlet-extracted, first with toluene (for 12 h) and then with dichloromethane (for 12 h). The light brown material thus prepared was dried at 353 K for 12 h. Sulfonic acid functional group = 0.38 mmol/g silica (estimate based on sulfur analysis). $Mn(Salen)^+$ (estimated by AAS) = 0.16 mmol/g silica.

2.1.5. Preparation of SBA-15-Mn(Salen)

In a typical preparation, 2 g of calcined SBA-15 (activated at 373 K for 4 h) was dispersed in 30 ml of dry-toluene and 0.3 g of Mn(Salen)Cl was added to it. The contents were refluxed under nitrogen for 24 h. The solid was separated, Soxhlet extracted with toluene followed by dichloromethane, and then dried at 353 K. $Mn(Salen)^+$ (estimated by AAS) = 0.07 mmol/g.

2.1.6. Zeolite-Y-encapsulated Mn(Salen)

The zeolite-Y-encapsulated $Mn(Salen)^+$ (hereafter referred to as Mn(Salen)-Y) was prepared according to reported procedures [18] employing the flexible ligand synthesis method. Mn content (AAS) = 0.31 mmol/g.

2.2. Materials characterization

X-ray diffractograms were recorded on an X'Pert Pro (Philips) diffractometer using Cu Kα radiation and a proportional counter as detector. A divergence slit of 1/32° on the primary optics and an anti-scatter slit of 1/16° on the secondary optics were employed to measure data in the low-angle region. Transmission electron micrographs (TEM) of the samples were scanned on a JEOL (model 1200 EX) microscope operating at 100 kV. The samples for TEM were dispersed in isopropyl alcohol, deposited on a Cu-grid and dried. Metal ion contents in the solid catalysts were estimated by atomic absorption spectroscopy (AAS). The C, H, N and S composition was determined by a Carlo-Erba 1106 analyzer. The specific surface area (BET) of the samples was determined using a NOVA 1200 Quanta Chrome instrument. The data points of p/p_0 in the range of about 0.05–0.3 were used in the calculations. The micropore volume was estimated from the *t*-plot and the pore diameter was estimated using the Barret–Joyner–Halenda (BJH) model. Thermogravimetric analysis was done on a Seiko DTA–TG 320 instrument under air (50 ml/min), at a ramp rate of 10 K/min, in the temperature range of 308–1078 K. FT-IR spectra were recorded on a Shimadzu 8201 PC spectrophotometer in the region 400–4000 cm^{-1}. Diffuse-reflectance UV–vis (DRUV–vis) spectra were obtained with a Shimadzu UV-2500 PC spectrophotometer in the range 200–850 nm. Electron paramagnetic resonance (EPR) measurements were done at 298 K using a Bruker EMX X-band (ν = 9.78 GHz) spectrometer with a 100 kHz field-modulation.

2.3. Reaction procedure

Oxidation of *R*-(+)-limonene over Mn(Salen) complexes with air as oxidant was carried out in a double-necked round bottom flask at atmospheric pressure and room temperature (298 K). In a typical reaction, known quantities of catalyst

(“neat” Mn(Salen)Cl: 0.0165 g or immobilized Mn(Salen) complex: 0.1 g), *R*-(+)-limonene (3.75 mmol), *iso*-butyraldehyde (9 mmol), an additive such as imidazole (Im), *N*-methylimidazole (*N*-MeIm) or 2-methylimidazole (2-MeIm) (1.7 mmol) and solvent (toluene, dichloromethane, acetonitrile, acetone, *tert*-butanol or methanol) (20 ml) were combined and the reaction was conducted by bubbling air at atmospheric pressure. The liquid samples were withdrawn at fixed time intervals and analyzed by gas chromatography (Varian 3400; CP-SIL8CB column; 30 m long and 0.53 mm i.d.). The products were identified using standard samples and by GC–MS (Shimadzu QP-5000; 30 m long, 0.25 mm i.d., and 0.25 μm thick capillary column DB-1).

3. Results and discussion

3.1. Catalyst characterization

3.1.1. Chemical analysis

Sulfonic acid-functionalized SBA-15 molecular sieves were prepared by the secondary synthesis route using the protocol shown in Scheme 1: in the first step, thiol-functionalized SBA-15 (SBA-15-*pr*-SH) was prepared by silylation/condensation of pre-formed, vacuum-dried SBA-15 with MPTMS, which was then, in the second step, oxidized with aqueous H_2O_2 to the sulfonic acid functionality (SBA-15-*pr*-SO_3H). As the materials possess ion-exchange capacity [16], $Mn(Salen)^+$ ions could be readily immobilized on the functionalized SBA-15 surface (Scheme 1). Chemical analysis (Table 1) revealed that SBA-15-*pr*-SO_3H contained 0.31 mmol of –*pr*-SO_3H groups per gram silica. Out of this, 0.16 mmol participated in coordination with $Mn(Salen)^+$ ions (as estimated by AAS). Mn(Salen) could also be immobilized directly on “bare” SBA-15 surfaces. However, the amount immobilized was low (0.07 mmol as against 0.16 mmol/g silica in the case of SBA-15-*pr*-SO_3-Mn(Salen)); even this low amount was leached out readily during the oxidation reactions. The organic functional groups have three potential sites (–$Si(OCH_3)_3$) that can bind to the silica surface. While all the three –Si–OCH_3 can, in principle, react with surface silanol groups to form Si–O–Si bonds, as suggested in Scheme 1, it is also possible that only one or two of the alkoxy groups would react with surface silanol groups. In addition, two of the SH-propyltrimethoxysilane molecules may also react with each other, forming direct Si–O–Si bonds between the organic functional molecules. However, at the low concentrations of functional groups utilized in the present case, such a possibility and the formation of disulfide bonds are unlikely. Spectral analysis did not indicate the presence of such disulfide bonds.

3.1.2. Structural and textural properties

SBA-15 and its functionalized derivatives showed XRD peaks in the 2θ range of 1–2.3° (Fig. 1) attributable to 2D hexagonal *p6mm* symmetry [15,16]. The well-resolved (1 1 0) and (2 0 0) reflections reveal long-range, mesopore ordering typical of SBA-15. Upon metal complex immobilization, the XRD peaks broadened and shifted marginally (by 0.06°) to higher 2θ values. The d spacing (d_{100}) and unit cell parameters, estimated from the position of the low-angle (1 0 0) peak, are in the range of 9.1–9.9 nm and 10.6–11.5 nm, respectively. These values agree well with those reported by others [15,16]. Transmission electron micrographs (Fig. 2) confirm the 2D hexagonal pore arrangement and the long-range mesoporous architecture. Organic functionalization and metal complex immobilization thus have little effect on the long-range mesoporous ordering.

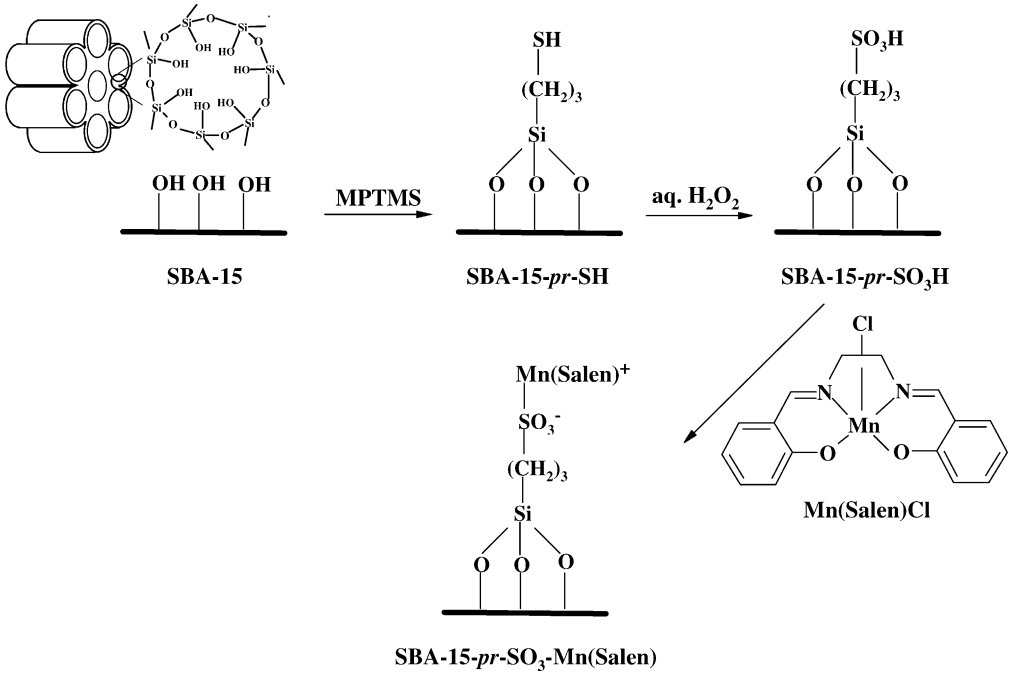

Scheme 1. Procedure for immobilization of $Mn(Salen)^+$ complexes on sulfonated SBA-15.

Table 1
Chemical composition and structural properties of immobilized Mn(Salen) complexes

System	Chemical composition (wt.%)[a]					Organic functional group (mmol/g solid catalyst)[b]	Immobilized Mn(Salen) complex (mmol/g solid catalyst)[c]	XRD		N_2 adsorption			Wall thickness (nm)
	C	H	N	S	Mn			d_{100} (nm)[d]	Unit cell parameter (nm)[d]	Pore diameter (nm)[e]	S_{BET} (m^2/g)	Total pore volume (cm^3/g)	
SBA-15	0.4	0.9	0	0	0	0	0	9.5	11.0	5.1	769	0.98	5.8
SBA-15-*pr*-SH	6.3	1.8	0	4.7	0	1.5	0	9.9	11.5	5.2	440	0.57	6.3
SBA-15-*pr*-SO_3H	4.8	1.8	0	1.8	0	0.56	0	9.7	11.3	6.7	539	0.64	4.5
SBA-15-*pr*-SO_3-Mn(Salen)	7.9	2.2	1.1	1.0	0.9	0.31	0.16	9.1	10.6	6.7	289	0.47	3.9
SBA-15-Mn(Salen)	2.9	0.9	[f]	–	0.4	–	0.07	10.3	11.9	–	–	–	–
Mn(Salen)Cl-Y	6.7	2.2	1.5	–	1.7	–	0.31	–	–	3.2	347	0.03	
"Neat" Mn(Salen)Cl	53.0	4.6	8.5	0	2.6	–	–	–	–	–	–	–	–

[a] C, H, N and S were estimated by elemental analysis. Mn was estimated by AAS.
[b] Determined based on S-content.
[c] Determined based on Mn-content.
[d] X-ray radiation is Co Kα except for SBA-15-Mn(Salen) where Cu Kα radiation was used.
[e] Determined using the BJH model.
[f] Below the instrumental detection limit.

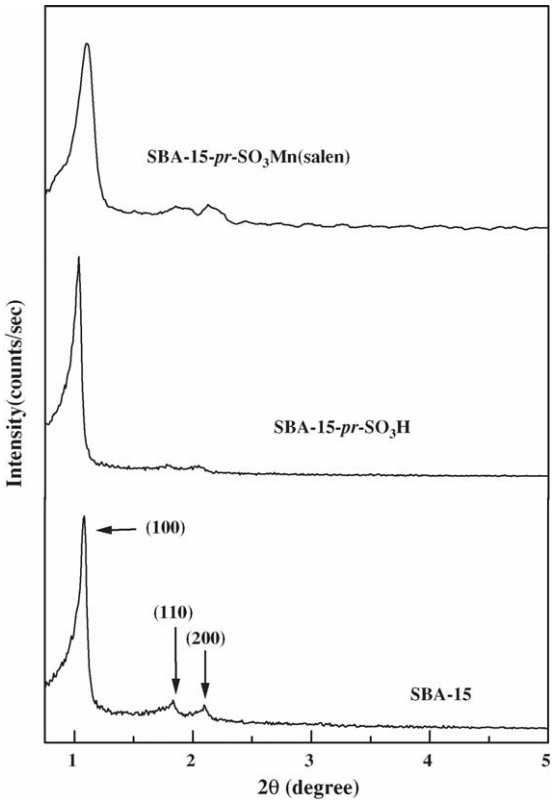

Fig. 1. XRD patterns of SBA-15 and functionalized materials.

SBA-15 was characterized by type IV nitrogen adsorption–desorption isotherms with H1 hysterisis (Fig. 3). Upon organic functionalization, marked decreases in BET surface area (from 539 to 289 m^2/g) and total pore volume (from 0.64 to 0.47 cm^3/g) (Table 1) were observed. The pore diameters were in the range of 5.1–6.7 nm, corresponding to those of mesoporous materials.

3.1.3. Spectral properties

SBA-15 showed characteristic FT-IR peaks at around 1040–1260, 820 and 500 cm^{-1} due to Si–O–Si stretching vibrations and a broad, asymmetric feature at 2900–3800 cm^{-1} due to O–H of silanols and water (Fig. 4(a)). Functionalization with –*pr*-SH showed additional features at 2928 and 2852 cm^{-1} due to C–H stretching vibrations and a weak peak at 2575 cm^{-1}, confirming the presence of SH functionality [15]. In the case of SBA-15-*pr*-SO_3H, the band at 2575 cm^{-1} was absent, indicating that the –SH functionalities originally present in SBA-15-*pr*-SH were oxidized to –SO_3H (bands at 650 and 1060 cm^{-1}) in SBA-15-*pr*-SO_3H [16].

"Neat" Mn(Salen)Cl showed characteristic IR bands at 1627, 1615, 1538, 1440, 1287 and 760 cm^{-1} (Fig. 4(b) and Table 2). These features, masked by the intense bands of the support, were only weakly visible in the supported materials due to the low concentration of Mn(Salen). Upon immobilization (on SBA-15, and zeolite-Y), the band at 1615 cm^{-1} due to ν(C=N) [17] in "neat" Mn(Salen)Cl shifted to 1602 cm^{-1} and the band at 1287 cm^{-1} corresponding ν(C–O) [17] shifted to 1296 cm^{-1}. The band at 760 cm^{-1} due to ring vibrations shifted

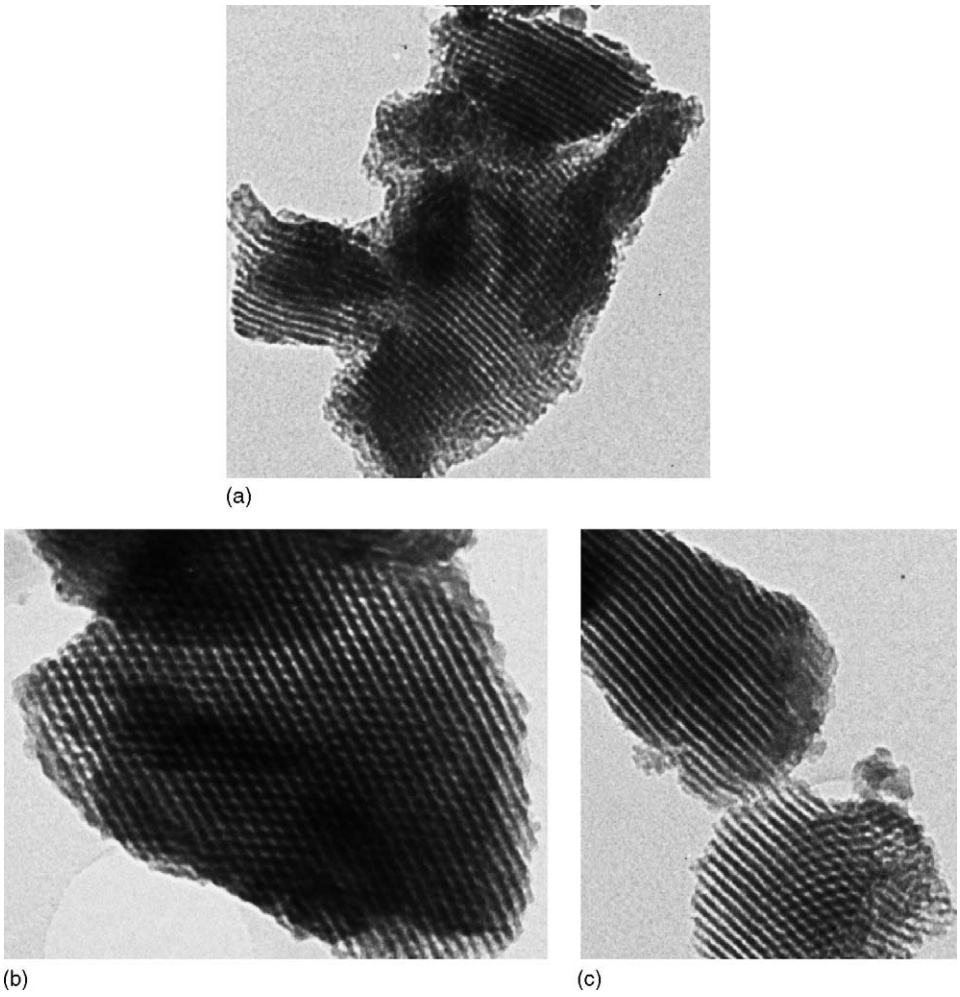

Fig. 2. Transmission electron micrographs: (a) SBA-15, (b) SBA-15-*pr*-SO_3H, and (c) SBA-15-*pr*-SO_3-Mn(Salen).

to 751 cm^{-1}. These shifts in band position can be attributed to molecular isolation and changes in conformation geometry of the Salen ligand [18,19]. Metal Salen complexes are known to exhibit different conformational geometries (planar, stepped and umbrella-shaped) depending on the counter ion, substituent in Salen ligand and solvent of crystallization [20].

The immobilized Mn(Salen) complexes exhibited several bands in the spectral region 200–600 nm (Fig. 5 and Table 2). The

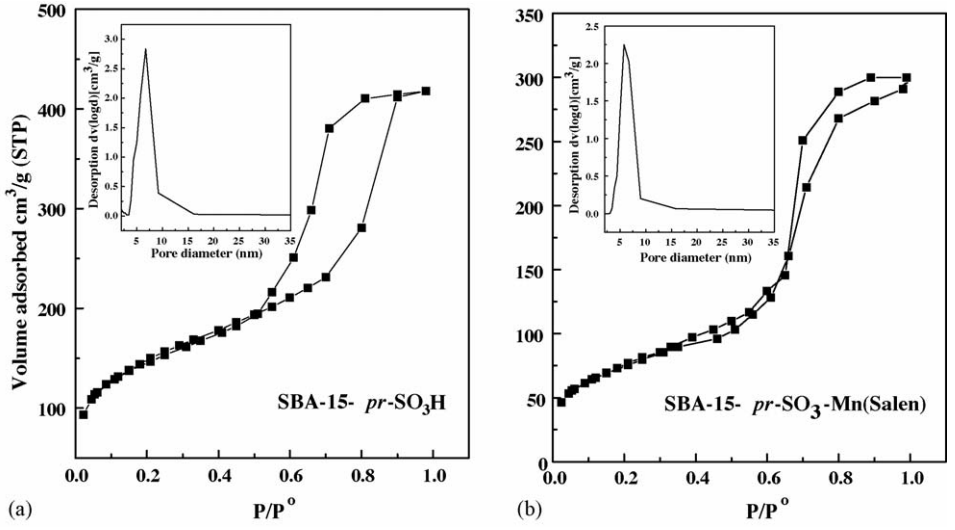

Fig. 3. N_2 adsorption–desorption isotherms of functionalized SBA-15 materials.

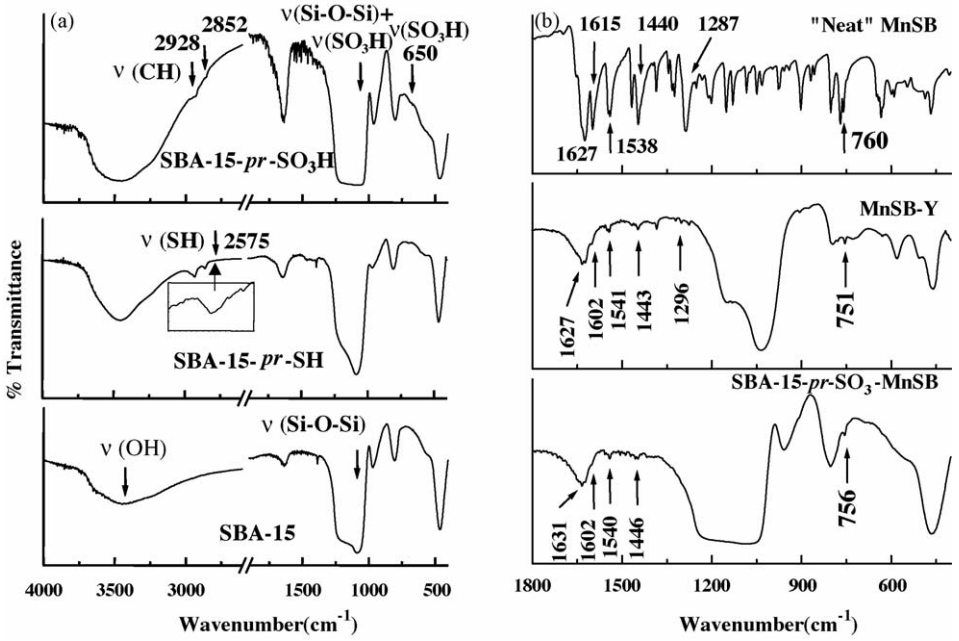

Fig. 4. FT-IR spectra of SBA-15, functionalized SBA-15 and ''neat'' and immobilized Mn(Salen) complexes.

band at 320 nm due to ligand-to-metal charge transfer transition (LMCT) [17,18,21], undergoes a blue shift to 310 nm upon immobilization. In addition, a shift in d–d bands from 425 and 500 nm (in ''neat'' Mn(Salen)Cl) [17,18,21] to 407 and 478 nm (in SBA-15-*pr*-SO_3-Mn(Salen)), respectively, was also noted.

''Neat'' Mn(Salen)Cl was EPR-silent, consistent with the +3 oxidation state of the Mn ions (Fig. 6, curve (a)). Mn(Salen) immobilized on the ''bare'' SBA-15 surface was also EPR-silent. However, the sulfonic acid-functionalized solid catalysts showed strong EPR signals characteristic of Mn^{2+} ions (Fig. 6, curve (c)). It may be recalled that both these solid catalysts were prepared using the same batch of ''neat'' Mn(Salen)Cl complex. The sulfonic acid groups present on the surface probably reduced the Mn ions in Mn(Salen) from +3 to +2. To test this hypothesis, ''neat'' Mn(Salen) complex was dissolved in sulfuric acid and its EPR spectrum was recorded. The sample became EPR active (Fig. 6, curve (b)) and intense signals similar to those observed for SBA-15-*pr*-SO_3-Mn(Salen) appeared. DRUV–vis and IR spectra reveal that the Schiff base Salen ligand is unaffected and not decomposed upon coordination to sulphonic acid groups. The charge transfer bands at 240, 285 and 350 nm (Fig. 5), the stretching frequency at 1627 cm^{-1} (Fig. 4 and Table 2), elemental analysis (Table 1) and thermal analysis (see the following section) clearly confirm that the Schiff base ligand and C=N groups are not affected on coordination with $–SO_3^-$. The $–SO_3^-$ group replaces the chloride ion present in the ''neat'' complex.

3.1.4. Thermal stability

Thermal analysis (TG–DTA) of SBA-15 (Fig. 7) showed three stages of weight loss, in agreement with the earlier reports [22]. Stage I (313–475 K; exothermic) corresponds to the loss of physically held water; stage II (475–815 K, exothermic) corresponds to the loss of water present within the micropore walls. Stage III (815–1273 K, endothermic) is due to silanol condensation ($2Si–OH \rightarrow Si–O–Si + H_2O$). SBA-15-*pr*-SH and SBA-15-*pr*-SO_3H showed four stages of weight loss: stages I, IIA, IIB and III, respectively. Stages IIA (475–661 K) and IIB (661–815 K) are due to desorption of water from the micropore walls as well as decomposition of the organic functional group (*–pr*-SH and *–pr*-SO_3H) [22]. SBA-15-*pr*-SO_3-Mn(Salen), on the other hand, showed five stages of weight losses: stages I, IIA, IIB, IIIA and IIIB, respectively. The additional weight losses in stages IIB and IIIA, IIIB (Table 2) are due to decomposition of the immobilized Salen complex.

3.2. Catalytic activity—oxidation of R-(+)-limonene

Oxidation of limonene can yield a variety of products (Scheme 2). The immobilized Mn(Salen) complexes, however, yielded the 1,2-epoxide with selectives greater than 90% at higher conversion levels (Table 3).

3.2.1. Influence of additives

The reaction did not occur in the absence of a catalyst or when *iso*-butyraldehyde (co-oxidation reagent) or the nitrogen-containing base (additive) was not used. With different N-containing bases, the catalytic activity of SBA-15-*pr*-SO_3-Mn(Salen) decreased in the order: *N*-MeIm > Im > 2-MeIm in parallel with the decreasing electron donor capability of the nitrogen-containing bases.

3.2.2. Effect of immobilization

SBA-15-*pr*-SO_3-Mn(Salen) (TOF = 17.8 h^{-1}) is considerably more active than Mn(Salen)-Y (TOF = 5.6 h^{-1}) or the ''neat'' complex (TOF = 7.0) (Table 3). The sulfonated catalysts also yielded a higher diasteriomeric excess (de) of 39.8% compared to 27.4% for the non-sulfonated analogs.

Table 2
Spectroscopic characteristics and thermal analysis of immobilized Mn(Salen) complexes

System	FT-IR (cm^{-1})[a]				UV–vis (nm)[b]				TG–DTA (weight loss, %)		
	ν(C=N)	ν(C=C)	Ring	ν(C–O)	SBA-15/Y	Salen	LMCT	d–d	Stage I 313–475 K (*exo*)	Stage II (A/B) 475–660 K and 660–815 K (*exo*)	Stage III (A/B) 815–1064 K and 1064–1273 K (*endo*)
SBA-15	–	–	–	–	210	–	–	–	2.35	4.14	2.09
SBA-15-*pr*-SH	–	–	–	–	210	–	–	–	1.08	12.62, 2.94	3.28
SBA-15-*pr*-SO_3H	–	–	–	–	210, 260	–	–	–	3.71	6.46, 4.96	4.34
SBA-15-*pr*-SO_3-Mn(Salen)	1631, 1602	1540	1464, 1446, 756	–	210	243, 285, 350	312	407, 478	3.71	6.46, 8.73	4.44, 1.39
SBA-15-Mn(Salen)	1628	1544	1459	–	–	236, 285, 350	313	400, 486	–	–	–
Mn(Salen)-Y	1627, 1602	1541	1467, 1443, 751	1296	–	241, 285, 350	321	422	–	–	–
"Neat" Mn(Salen)Cl	1627, 1615	1538	1468, 1440, 760	1287	–	240, 285, 350	320	425, 500	–	–	–

[a] As KBr pellets.
[b] Data for "neat" Mn(Salen)Cl corresponds to that for CH_2Cl_2 solutions. For the rest of the samples (measurement in diffused reflectance mode) spectral grade $BaSO_4$ was used as the reference.

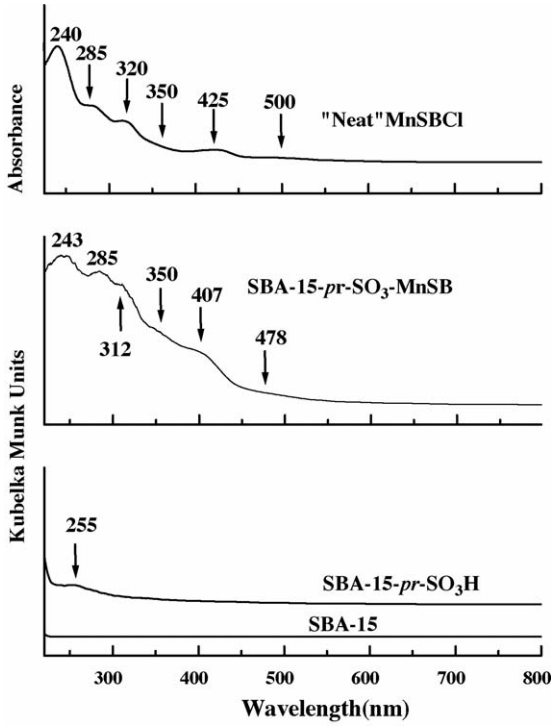

Fig. 5. UV–vis spectra of SBA-15, SBA-15-*pr*-SO_3H and SBA-15-*pr*-SO_3-Mn(SB) in diffuse reflectance mode and "neat" Mn(SB)Cl in CH_2Cl_2 in normal absorption mode. SB refers to Salen.

3.2.3. Influence of solvent

The catalytic activity of SBA-15-*pr*-SO_3-Mn(Salen) in different solvents decreased in the order: toluene > acetonitrile > acetone > dichloromethane (Table 4). The reaction did not proceed when alcohols (methanol and *tert*-butanol) were

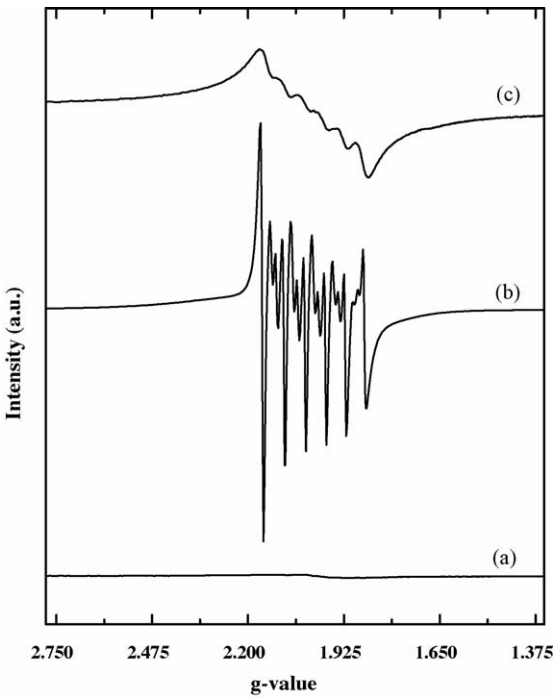

Fig. 6. EPR spectra (9.45 GHz, 90 K) of (a) "neat" Mn(Salen)Cl, (b) "neat" Mn(Salen)Cl dissolved in H_2SO_4, and (c) SBA-15-*pr*-SO_3-Mn(Salen).

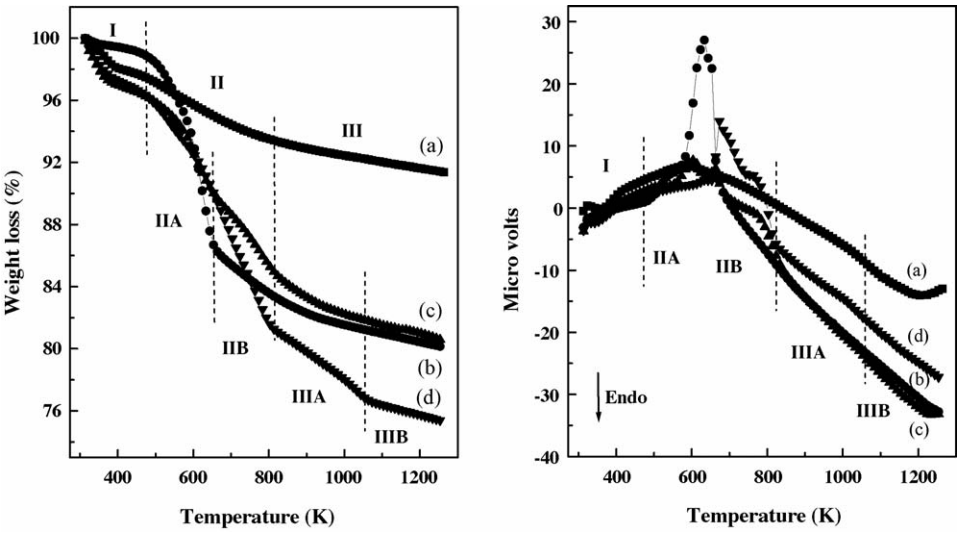

Fig. 7. TGA and DTA profiles: (a) SBA-15, (b) SBA-15-*pr*-SH, (c) SBA-15-*pr*-SO_3H, and (d) SBA-15-*pr*-SO_3-Mn(Salen).

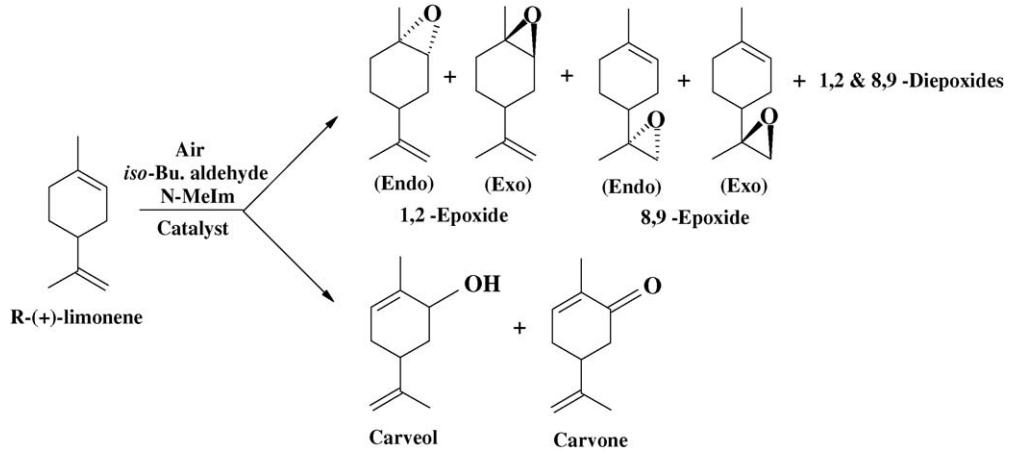

Scheme 2. Oxidation of limonene and the possible oxidation products.

Table 3
Aerial oxidation of *R*-(+)-limonene over immobilized Mn(Salen) complexes[a]

Catalyst	Additive	Conversion of *R*-(+)-limonene (mol%)	TOF (h^{-1})[b]	Product selectivity (%)					Diasterio-meric excess (de)[c]
				1,2-Epoxide	8,9-Epoxide	1,2- and 8,9-diepoxide	Carveol	Carvone	
"Neat" Mn(Salen)Cl	*N*-MeIm	69.2	7.0	74.2	7.2	6.2	5.2	7.2	35.8
SBA-15-*pr*-SO_3-Mn(Salen)	*N*-MeIm	60.0	17.8	82.0	8.0	2.6	3.7	3.7	39.8
SBA-15-*pr*-SO_3-Mn(Salen)	Im	29.8	9.0	94.2	5.8	0	0	0	
SBA-15-*pr*-SO_3-Mn(Salen)	2-MeIm	0.0	–	–	–	–	–	–	–
SBA-15-Mn(Salen)	*N*-MeIm	21.1	14.8	100	0	0	0	0	27.4
Mn(Salen)-Y	*N*-MeIm	36.8	5.6	97.7	2.3	0	0	0	35.8

[a] Reaction conditions: *R*-(+)-limonine = 3.75 mmol; *iso*-butyraldehyde = 9 mmol; additive = 1.7 mmol; catalyst = 0.0165 g ("neat" Mn(Salen)Cl) and 0.1 g (rest of the catalysts); solvent—toluene = 20 ml; oxidant: air (1 atm); reaction temperature = 298 K; reaction time = 8 h. *N*-MeIm: *N*-methyl imidazole; Im: imidazole, 2-MeIm: 2-methylimidizole.

[b] Turnover frequency (TOF) = Moles of *R*-(+)-limonene converted per mole of Mn per hour.

[c] Diasteriomeric excess (de) = (% selectivity of *endo*-1,2-epoxide − % selectivity of *exo*-1,2-epoxide) × 100/(% total 1,2-epoxide selectivity).

Table 4
Influence of solvent on aerial oxidation of *R*-(+)-limonene over SBA-15-*pr*-SO_3-Mn(Salen)[a]

Solvent	Conversion of *R*-(+)-limonene (mol%)	TOF (h^{-1})[b]	Product selectivity (%)				
			1,2-Epoxide	8,9-Epoxide	1,2- and 8,9-diepoxide	Carveol	Carvone
Toluene[c]	60.0	17.8	82.0	8.0	2.6	3.7	3.7
Dichloromethane	9.4	2.8	100	0	0	0	0
Acetonitrile	39.2	11.8	100	0	0	0	0
Acetone	27.1	8.1	100	0	0	0	0

[a] Reaction conditions: *R*-(+)-limonine = 3.75 mmol; *iso*-butyraldehyde = 9 mmol; additive—*N*-MeIm = 1.7 mmol; catalyst = 0.1 g; solvent = 20 ml; oxidant: air (1 atm); reaction temperature = 298 K; reaction time = 12 h.
[b] Turnover frequency (TOF) = Moles of *R*-(+)-limonene converted per mole of Mn per hour.
[c] Reaction time = 8 h.

used as solvent. Alcoholic solvents probably compete with the nitrogen bases for coordination to Mn ions and thereby retard the catalytic activity.

3.2.4. Influence of reaction time

Conversion of limonene increased with time and reached a maximum at 8 h. 1,2-Epoxide was the only product at lower conversions. At conversions above 20%, 8,9-epoxide and 1,2- and 8,9-diepoxides were also formed. At conversions above 50%, carveol and carvone formed in smaller quantities in addition to the epoxide. At similar conversions, the encapsulated complexes yielded the *endo*-1,2-epoxide more selectively (Fig. 8).

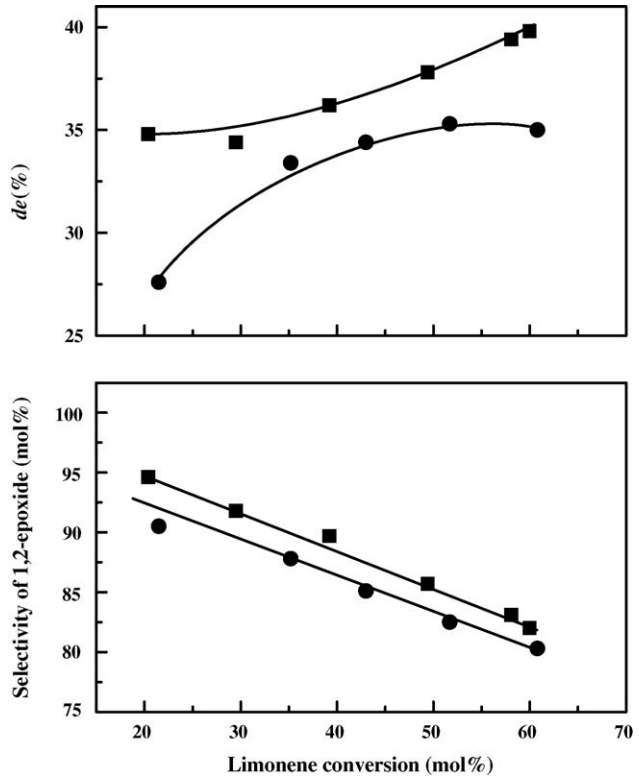

Fig. 8. Diastereomeric excess (de) and 1,2-epoxide selectivity as a function of limonene conversion over ''neat'' Mn(Salen)Cl (●) and SBA-15-*pr*-SO_3-Mn(Salen) (■).

The solid catalysts were hot-filtered at 2.5 h and the reaction was continued (Fig. 9). We found that limonene oxidation continued even after the catalyst was separated out. Analysis of the filtrate for metal ions by atomic absorption spectroscopy revealed that leaching of a part of the Mn ions had occurred. The solid catalyst was filtered and reused after washing with toluene and dichloromethane, followed by drying at 353 K for 2–4 h. While the diastereomeric selectivity (de value) was unaffected, the catalytic activity of SBA-15-*pr*-SO_3-Mn(Salen) decreased from 60% (for ''fresh'' catalyst) to 44% in the 5th recycle (Fig. 10). In the case of Mn(Salen)-Y, this decrease was from 36.8% to 20.3%. Mn(Salen) immobilized directly on ''bare'' SBA-15 became completely inactive in the 3rd recycle itself. A change in the oxidation state of Mn from +3 in the ''neat'' complex to +2 when immobilized on the sulfonated surface was inferred from EPR spectral studies. This change in the Mn ion oxidation state is a probable cause for the observed

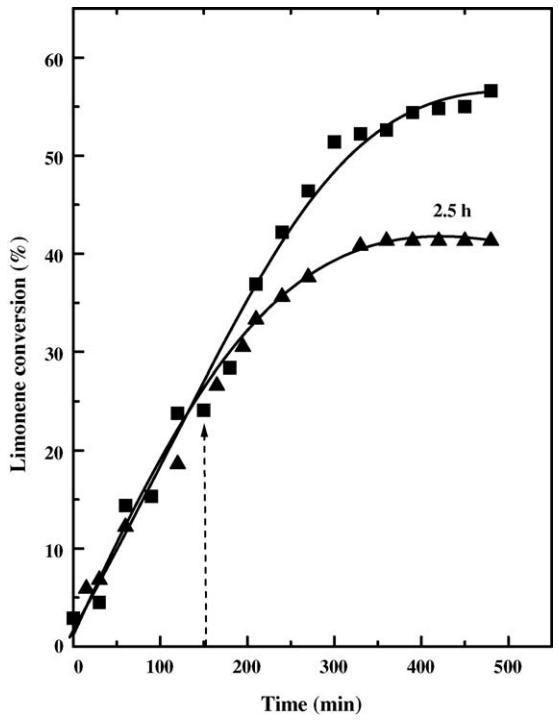

Fig. 9. Catalyst stability studies in limonene oxidation: catalyst—(SBA-15-*pr*-SO_3-Mn(Salen).

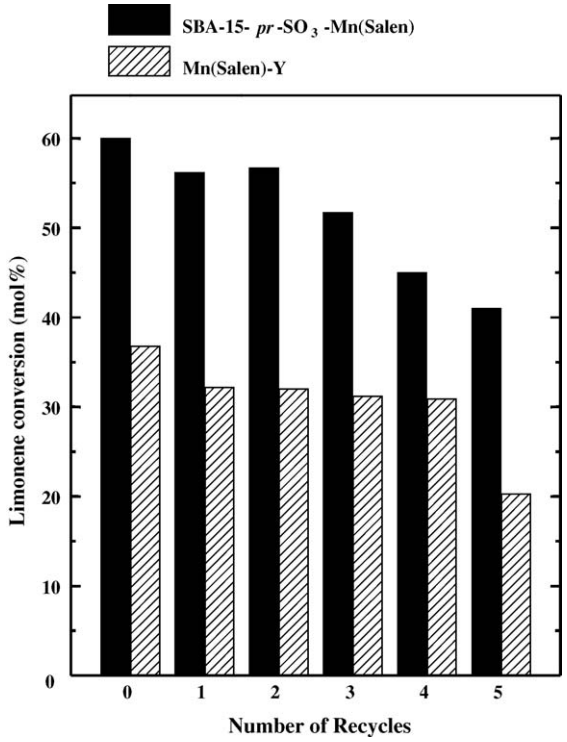

Fig. 10. Stability and reusability of immobilized Mn(Salen) complexes in limonene oxidation with air.

enhancement of catalytic activity of the immobilized Mn(Salen) complexes. The solid catalysts of the present study (SBA-15-*pr*-SO_3-Mn(Salen)) are more active and selective (epoxide selectivity 80% under the conversion 60% and the de 40%) than the related metal complexes reported in the literature [2–12].

4. Conclusions

Mn(Salen) complexes immobilized on sulfonic acid-functionalized SBA-15 exhibited efficient catalytic activity for selective epoxidation of *R*-(+)-limonene with aerial oxygen. 1,2-Limonene epoxide was the major product. The diastereomeric excess for the *endo*-enantiomer was 39.8%. The Mn complexes immobilized on the sulfonated surface showed more enhanced catalytic activity than the ''neat'' complexes and zeolite-Y-encapsulated Mn(Salen). Immobilization modified the oxidation state of Mn and the conformational geometry of the complex, thereby increasing their catalytic activity. The active sites were also better dispersed and more easily accessible for the substrate molecules in the case of sulfonic acid-functionalized, mesoporous SBA-15 than in zeolite-Y. The catalysts were, however, not stable during the oxidation reaction; Mn ions were leached out of the solid phase during the reaction.

Acknowledgments

L.S. acknowledges the University Grants Commission (UGC), New Delhi for a Junior Research Fellowship. We thank Mrs. N.E. Jacob, Mrs. Renu Pasricha and Mr. R. Jha for their help in the analyses.

References

[1] B.D. Mookherjee, R.A. Wilson, 4th ed., Encyclopedia of Chemical Technology Kirk-Orthmer, vol. 17, Wiley, New York, 1996, pp. 603–674.
[2] R. Hutter, T. Mallat, A. Baiker, J. Catal. 153 (1995) 177–189.
[3] (a) M.V. Cagnoli, S.G. Casuscelli, A.M. Alvarez, J.F. Bengoa, N.G. Gallegos, N.M. Samaniego, M.E. Crivello, G.E. Ghione, C.F. Pérez, E.R. Herrero, S.G. Marchetti, Appl. Catal. A: Gen. 287 (2005) 227–235; (b) M.V. Cagnoli, S.G. Casuscelli, A.M. Alvarez, J.F. Bengoa, N.G. Gallegos, M.E. Crivello, E.R. Herrero, S.G. Marchetti, Catal. Today 107/108 (2005) 397–403; (c) H.E.B. Lempers, R.A. Sheldon, Appl. Catal. A: Gen. 143 (1996) 137–143.
[4] (a) L.S. Salles, J.-Y. Piquemal, R. Thouvenot, C. Minot, J.-M. Brégeault, J. Mol. Catal. A: Chem. 117 (1997) 375–387; (b) M.A. Armendía, V. Borau, C. Jiménez, J.M. Luque, J.M. Marinas, J.R. Ruiz, F.J. Urbano, Appl. Catal. A: Gen. 216 (2001) 257–265; (c) P.A.L. Villa, A.F. Taborda, C. Monte de Correa, J. Mol. Catal. A: Chem. 185 (2002) 269–277; (d) N.K. Kala Raj, V.G. Puranik, C. Gopinathan, A.V. Ramaswamy, Appl. Catal. A: Gen. 256 (2003) 265–273; (e) S. Casuscelli, E. Herrero, M. Crivello, C. Pérez, M.G. Egusquiza, C.I. Cabello, I.L. Botto, Catal. Today 107/108 (2005) 230–234.
[5] (a) L.E. Firdoussi, A. Baqqa, S. Allaoud, B.A. Allal, A. Karim, Y. Castanet, A. Mortreux, J. Mol. Catal. A: Chem. 135 (1998) 11–22; (b) A.D. Silva, M.L. Patitucci, H.R. Bizzo, E. D'Elia, O.A.C. Antunes, Catal. Commun. 3 (2002) 435–440; (c) J. Bussi, A. López, F. Peña, P. Timbal, D. Paz, D. Lorenzo, E. Dellacasa, Appl. Catal. A: Gen. 253 (2003) 177–189; (d) P.A. Robles-Dutenhefner, D.L. Nunes, J.A. Gonçalves, E.V. Gusevskaya, E.M.B. Sousa, J. Non-Cryst. Solids 348 (2004) 195–200.
[6] P.A. Robles-Dutenhefner, M.J. da Silva, L.S. Sales, E.M.B. Sousa, E.V. Gusevskaya, J. Mol. Catal. A: Chem. 217 (2004) 139–144.
[7] (a) C. Schuster, W.F. Hölderich, Catal. Today 60 (2000) 193–207; (b) W.F. Hölderich, Catal. Today 62 (2000) 115–130.
[8] F.C. Skrobot, A.A. Valente, G. Neves, I. Rosa, J. Rocha, J.A.S. Cavaleiro, J. Mol. Catal. A: Chem. 201 (2003) 211–222.
[9] S. Tangestaninejad, M. Moghadam, V. Mirkhani, H. Kargar, Ultrason. Sonochem. 13 (2006) 32–36.
[10] P. Oliveira, A.M. Ramos, I. Fonseca, A. Botelho do Rego, J. Vital, Catal. Today 102/103 (2005) 67–77.
[11] S. Bhattacharjee, T.J. Dines, J.A. Anderson, J. Catal. 225 (2004) 398–407.
[12] (a) P.C. Bakala, E. Briot, L. Salles, J.M. Brégeault, Appl. Catal. A: Gen. 300 (2006) 91–99; (b) R. Raja, G. Sankar, J.M. Thomas, Chem. Commun. (1999) 829–830.
[13] (a) S. Borocci, F. Marotti, G. Mancini, D. Monti, A. Pastorini, Langmuir 17 (2001) 7198–7203; (b) L.F. Lima, L. Cardozo-Filho, P.A. Arroyo, H. Márquez-Alvarez, O.A.C. Antunes, React. Kinet. Catal. Lett. 84 (2005) 69–77; (c) B.B. Wentzel, P.L. Alsters, M.C. Feiters, R.J.M. Nolte, J. Org. Chem. 69 (2004) 3453–3464; (d) M.F.T. Gomes, O.A.C. Antunes, Catal. Lett. 42 (1996) 213–215.
[14] D. Zhao, J. Feng, Q. Huo, N. Melosh, G.H. Fredrickson, B.F. Chmelka, G.D. Stucky, Science 279 (1998) 548–552.
[15] (a) F. Feng, G.E. Fryxell, L.-Q. Wang, A.Y. Kim, K.M. Kemner, Science 276 (1997) 923–926; (b) L. Mercier, T.J. Pinnavaia, Adv. Mater. 9 (1997) 500–503; (c) A. Stein, B.J. Melde, R.C. Schroden, Adv. Mater. 12 (2000) 1403–1419; (d) T. Kang, Y. Park, J.C. Park, Y.S. Cho, J. Yi, Stud. Surf. Sci. Catal. 146 (2003) 527–530; (e) T. Kang, Y. Park, J. Yi, Ind. Eng. Chem. Res. 43 (2004) 1478–1484; (f) C.M. Crudden, M. Sateesh, R. Lewis, J. Am. Chem. Soc. 127 (2005) 10045–10050.

[16] (a) W.M. Van Rhijn, D.E. De Vos, B.F. Sels, W.D. Bossaert, P.A. Jacobs, Chem. Commun. (1998) 317–318;
(b) D. Das, J.-F. Lee, S. Cheng, Chem. Commun. (2001) 2178–2179;
(c) E. Cano-Serrano, J.M. Campos-Martin, J.L.G. Fierro, Chem. Commun. (2003) 246–247;
(d) B.C. Wilson, C.W. Jones, Macromolecules 37 (2004) 9709–9714.
[17] (a) K. Srinivasan, P. Michaud, J.K. Kochi, J. Am. Chem. Soc. 108 (1986) 2309–2320;
(b) T. Matsushita, H. Kono, T. Shono, Bull. Chem. Soc. Jpn. 54 (1981) 2646–2651;
(c) R.H. Holm, G.W. Everret, A. Chakravorty, Prog. Inog. Chem. 7 (1966) 82–214.
[18] (a) T.H. Bennur, D. Srinivas, P. Ratnasamy, Micropor. Mesopor. Mater. 48 (2001) 111–118;
(b) S.P. Varkey, C. Ratnasamy, P. Ratnasamy, J. Mol. Catal. A: Chem. 135 (1998) 295–306;
(c) C.R. Jacob, S.P. Varkey, P. Ratnasamy, Micropor. Mesopor. Mater. 22 (1998) 465–474.
[19] S. Deshpande, D. Srinivas, P. Ratnasamy, J. Catal. 188 (1999) 261–269.
[20] (a) M.M. Bhadbhade, D. Srinivas, Inorg. Chem. 32 (1993) 5458–5466;
(b) M.M. Bhadbhade, D. Srinivas, Polyhedron 17 (1998) 2699–2711;
(c) M. Suzuki, T. Ishikawa, A. Harada, S. Ohba, M. Sakamoto, Y. Nishida, Polyhedron 16 (1997) 2553–2561;
(d) V.L. Pecoraro, W.M. Butler, Acta Cryst. C42 (1986) 1151–1154;
(e) A.R. Oki, D.J. Hodgson, Inorg. Chim. Acta 170 (1990) 65–73.
[21] (a) R.I. Kureshy, I. Ahmad, N.H. Khan, S.H.R. Abdi, K. Pathak, R.V. Jasra, Tetrahedron: Asymmetry 16 (2005) 3562–3569;
(b) H. Zhang, S. Kiang, J. Kiao, C. Li, J. Mol. Catal. A: Chem. 238 (2005) 175–184.
[22] (a) B. Sow, S. Hamoudi, M.H. Zahedi-Niaki, S. Kaliaguine, Micropor. Mesopor. Mater. 79 (2005) 129–136;
(b) L.M. Yang, Y.J. Wang, G.S. Luo, Y.Y. Dai, Micropor. Mesopor. Mater. 84 (2005) 275–282.